APPENDIX

Adaptive Pathfinding by Nucleokinesis during Amoeboid Migration

Authors: Janina Kroll[1], Robert Hauschild[2], Artur Kuznetcov[1], Kasia Stefanowski[1], Monika D. Hermann[1], Jack Merrin[2], Lubuna Shafeek[2], Annette Müller-Taubenberger[3], Jörg Renkawitz[1]*

Table of Contents:

Appendix Figure S1. Comparison of amoeboid nucleokinesis parameters to nucleokinesis in other cell types.

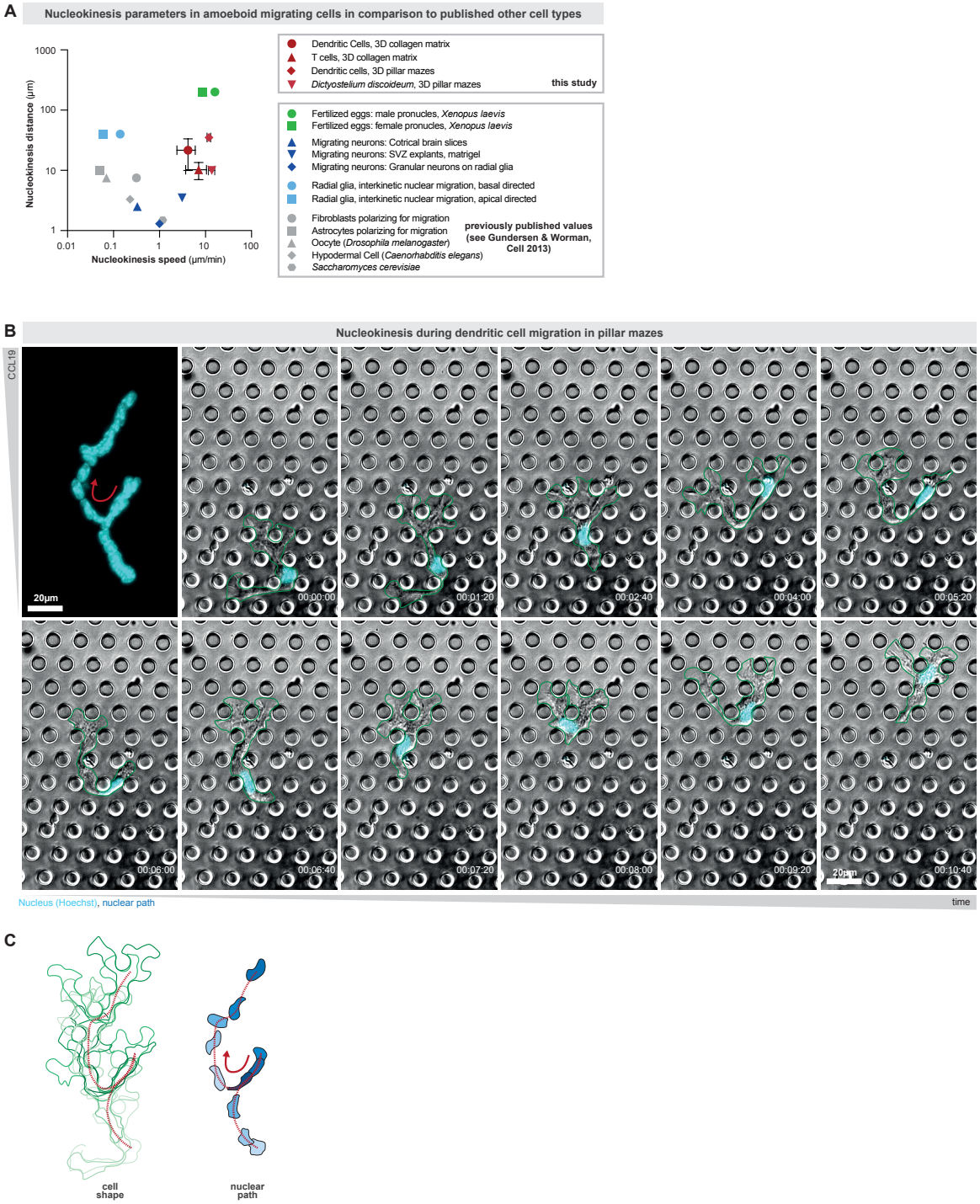

Appendix Figure S1. Comparison of amoeboid nucleokinesis parameters to nucleokinesis in other cell types.

A. Speed and distance of amoeboid nucleokinesis in dendritic cells, T cells, and *Dictyostelium discoideum*. Previously published nucleokinesis speeds and distances measured in other cell types are shown as a reference (Gundersen & Worman, Cell 2013). Data from this study are mean ±SD.

B. Representative bone marrow-derived dendritic cell (DC) migrating through a porous maze-like microenvironment composed of pillars interconnecting two surfaces below and above the migrating cell. The cell shape is outlined in green and the nucleus is visualized by Hoechst (cyan). Red arrow highlights nucleokinesis event. Time in hr:min:sec.

C. Time projections of the cellular and nuclear paths of the cell in B are shown in shades of green and blue, respectively. Red arrow highlights nucleokinesis event, and the red dashed line shows the nuclear path.

Appendix Figure S2. Novel reductionistic assay to characterize nucleokinesis during cell motility.

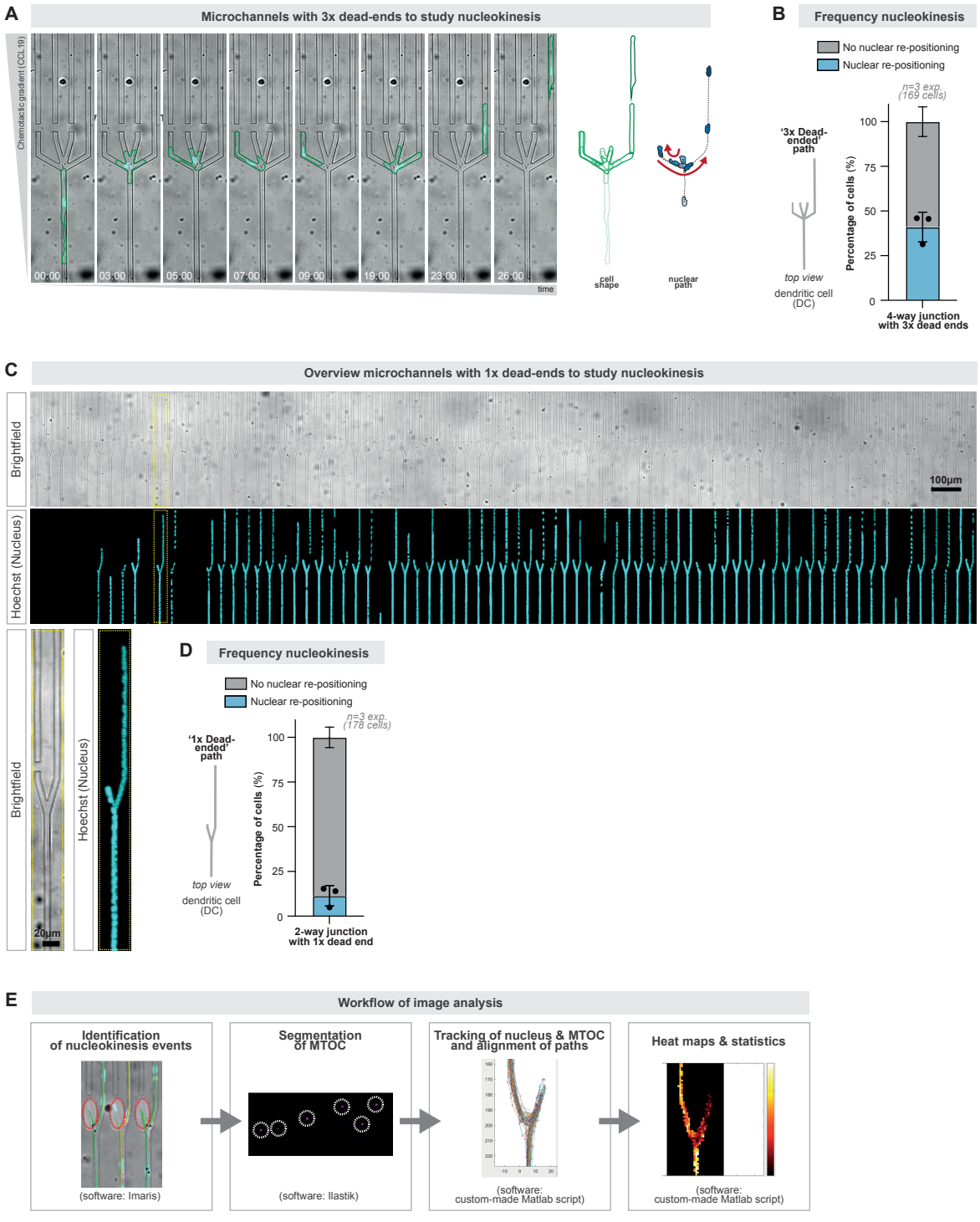

Appendix Figure S2. Novel reductionistic assays to characterize nucleokinesis during cell motility.

A. Representative bone marrow-derived DC (BMDC) migrating in a microchannel with a path junction that has one open and three blocked paths. Note the high frequency of nucleokinesis (nucleus in cyan; Hoechst) as quantified in B). To quantitively analyze the detailed spatio-temporal dynamics of nucleokinesis, we analyzed nucleokinesis in even more simple environments, in which cells approach path junctions that are composed of one dead-end path and one open continuous path (see C and D). The cellular shape and the position of the nucleus are outlined over time in shades of green and blue, respectively. Time in min:sec.

B. Quantification of the rate of nucleokinesis in a 4-way junction with 3x dead ends. N=3 replicates, 169 cells. Data are mean ±SD.

C. Overview of microchannels with 1x dead-end. Top: Brightfield, bottom: maximum projection of nuclear channel (Hoechst, cyan). The yellow-dotted regions are shown enlarged below.

D. Quantification of the rate of nucleokinesis in a 2-way junction with 1x dead end. N=3 replicates, 178 cells. Data are mean ±SD.

E. Workflow of semi-automated image analysis for cells migrating in the 2-junction with 1x dead end. Nucleokinesis events are identified by only selecting nuclear tracks entering a surface drawn manually over the dead end in Imaris. Ilastik is used to segment the MTOC signal. Subsequently, the nucleus and MTOC are tracked in Imaris. Using a custom-made Matlab script, tracks are aligned and heat maps and data on track speed, distance of nucleus and MTOC, and distance changes are generated.

Appendix Figure S3. Nucleus-to-MTOC distances and speeds during amoeboid nucleokinesis.

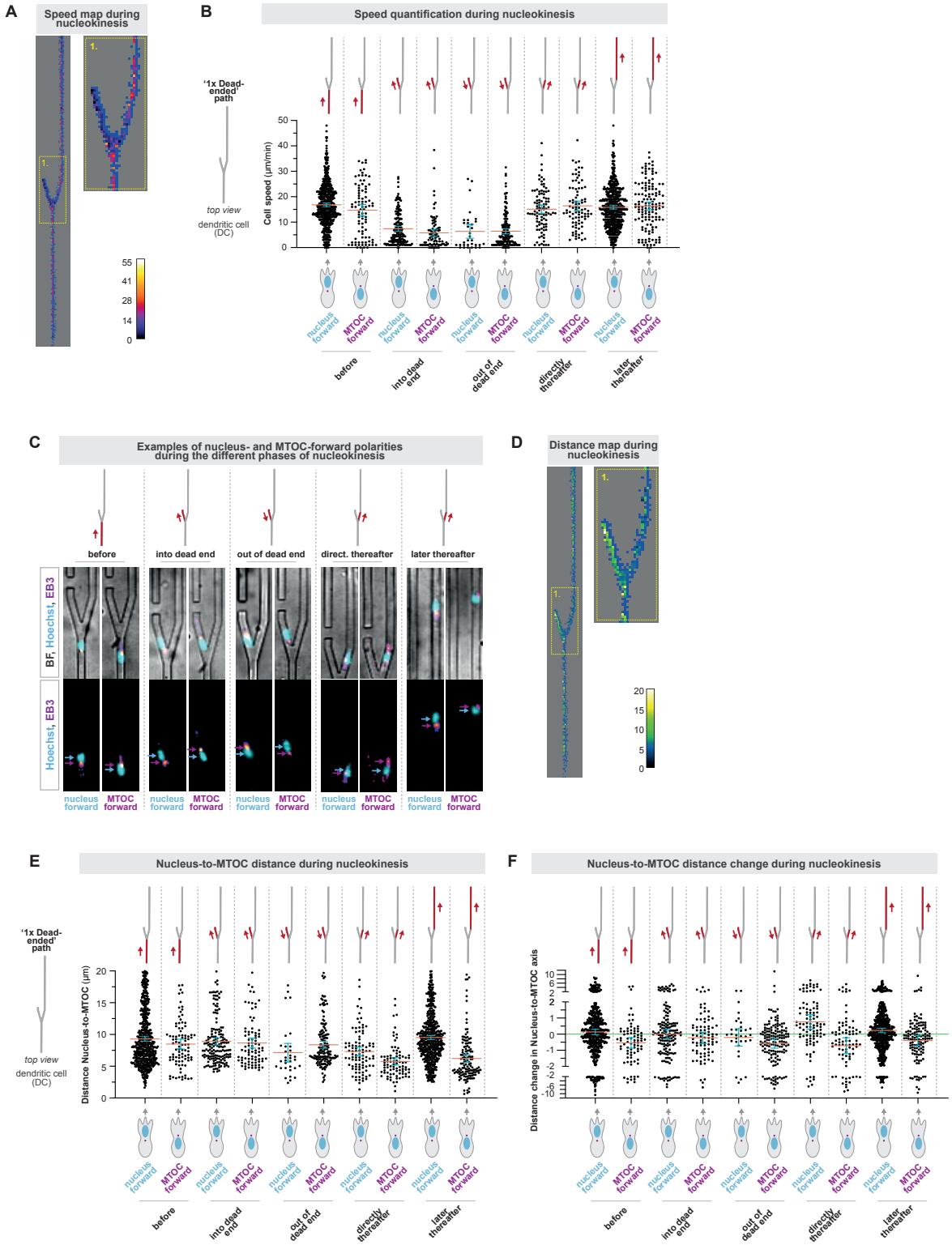

Appendix Figure S3. Nucleus-to-MTOC distances and speeds during amoeboid nucleokinesis.

A. Heatmap of nuclear speed during amoeboid nucleokinesis. The yellow-dotted region 1 is enlarged to depict the cellular behavior during the initial nucleokinesis event. N=6 replicates, 48 cells.

B. Quantification of nuclear speed during amoeboid nucleokinesis depending on the nucleus-MTOC axis configuration: EB3-mCherry expressing HoxB8-derived DCs, migrating through a path junction with one blocked path. The data show tracked nuclear velocities (visualized by Hoechst) of DCs that reposition their nucleus from the blocked to the open path by nucleokinesis. N=6 replicates, N=48 cells, total analyzed events per column (from 1st to last column): 566, 90, 165, 85, 32, 159, 96, 85, 541, 136; Data are mean ±95CI.

C. Distances between the MTOC and the nucleus during nucleokinesis in representative EB3-mCherry expressing Hoxb8-derived dendritic cells. See D) and E) for quantification of the distance, and F) for quantification of the distance change during the different phases of nucleokinesis.

D. Heatmap of the distance between nucleus and MTOC during amoeboid nucleokinesis. The yellow-dotted region 1 is enlarged to depict the cellular behavior during the initial nucleokinesis event. N=6 replicates, 48 cells.

E. Quantification of the distance between nucleus and MTOC during amoeboid nucleokinesis depending on the nucleus-MTOC axis configuration: EB3-mCherry expressing HoxB8-derived DCs, migrating through a path junction with one blocked path. The data show the distances between the center of the nucleus (visualized by Hoechst) and the center of the MTOC (visualized by EB3-mCherry) in DCs that reposition their nucleus from the blocked to the open path by nucleokinesis. N=6 replicates, N=48 cells, total analyzed events per column (from 1st to last column): 566, 90, 165, 85, 32, 159, 96, 85, 541, 136; Data are mean ±95CI.

F. Quantification of the nucleus-to-MTOC distance changes during amoeboid nucleokinesis depending on the nucleus-MTOC axis configuration: EB3-mCherry expressing HoxB8-derived DCs, migrating through a path junction with one blocked path. The data show the change of distances between the center of the nucleus (visualized by Hoechst) and the center of the MTOC (visualized by EB3-mCherry) in DCs that reposition their nucleus from the blocked to the open path by nucleokinesis. N=6 replicates, N=48 cells, total analyzed events per column (from 1st to last column): 566, 90, 165, 85, 32, 159, 96, 85, 541, 136; Data are mean ±95CI.

Appendix Figure S4. Consequences of low and high doses of nocodazole for the microtubule cytoskeleton and the velocity of migratory dendritic cells

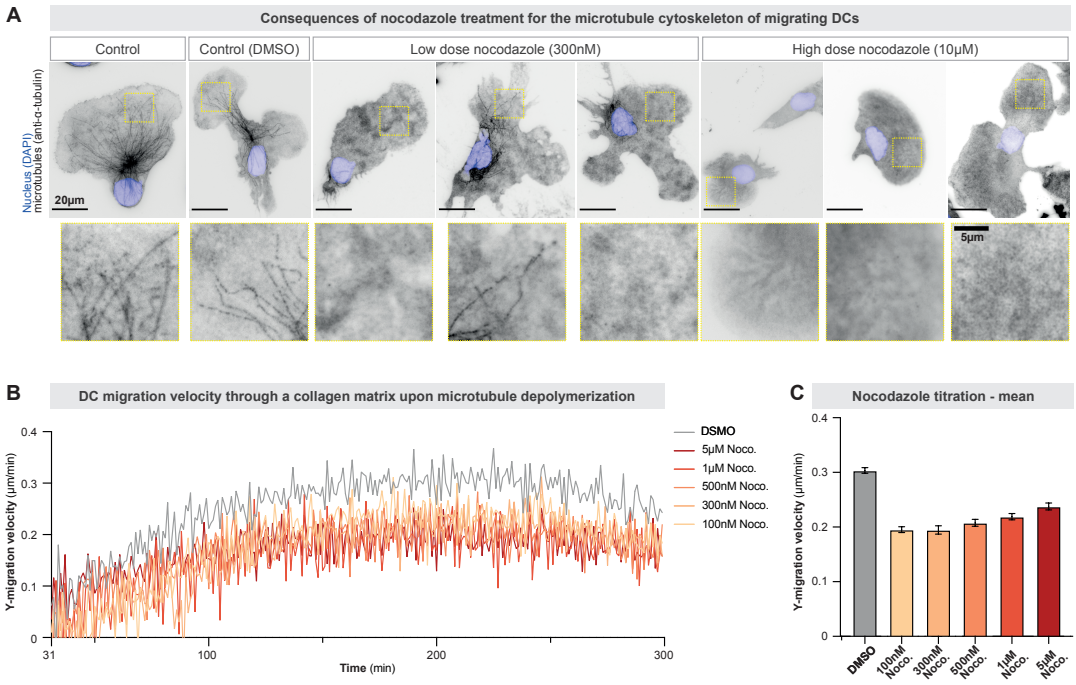

Appendix Figure S4. Consequences of low and high doses of nocodazole for the microtubule cytoskeleton and the velocity of migrating cells.

A. Immunofluorescence staining against alpha-tubulin (black) of DCs migrating in an under-agarose assay (Nucleus/DAPI shown in blue)**.** Note that microtubules typically reach far-distantly into at least one cellular protrusion in control cells (dashed yellow boxes show regions in the protrusions in an enlarged manner), whereas low doses of 300 nM nocodazole largely depolymerize the microtubule cytoskeleton in most cells, and high doses of 10 μM nocodazole entirely depolymerize the microtubule cytoskeleton.

B. Bone marrow-derived dendritic cell migration in three-dimensional (3D) collagen matrices (3.3 mg/ml) along a CCL19 chemokine gradient in the presence of different concentrations of Nocodazole (microtubule inhibitor) or DMSO (control). N=3 replicates. Data are mean.

C. Mean migration velocity between 150 and 250 min of cells shown in A. N=3 replicates. Data are mean ±95CI.

Appendix Figure S5. Reduced cell polarity switching during amoeboid nucleokinesis upon myosin-IIA knockout.

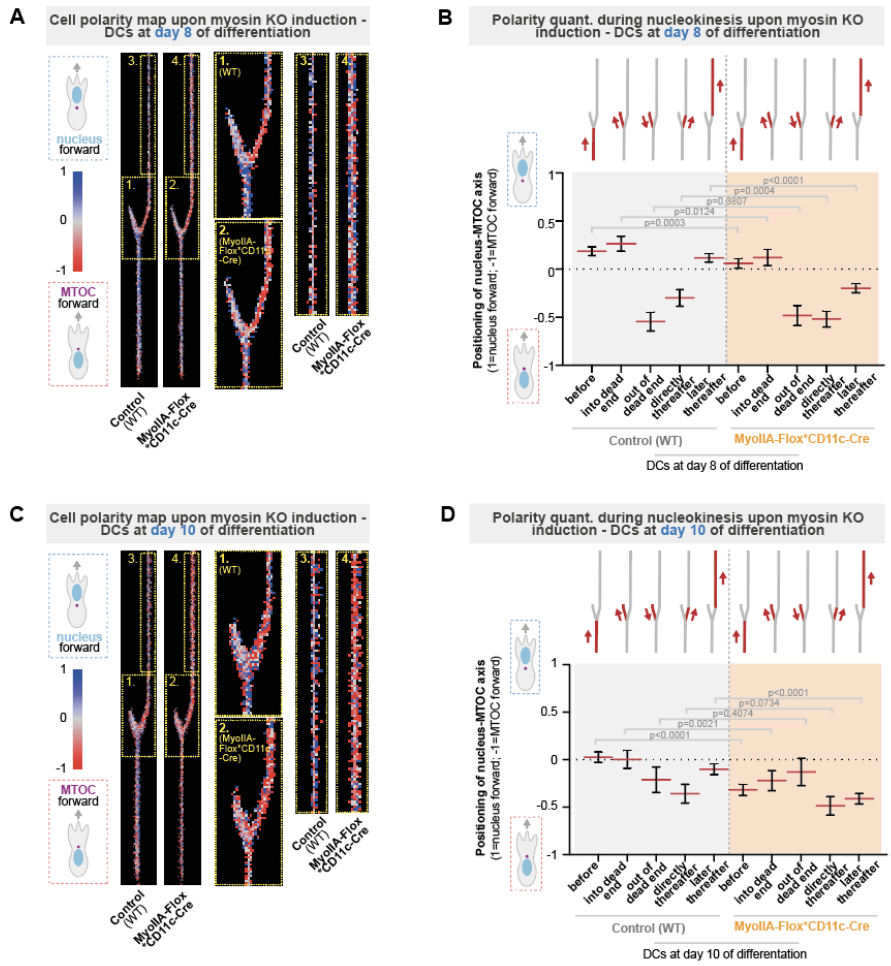

Appendix Figure S5. Reduced cell polarity switching during amoeboid nucleokinesis upon a conditional myosin-IIA knockout.

A. Heatmap of the nucleus-MTOC axis configuration during amoeboid nucleokinesis in myosin-IIA KO or control DCs at day 8 of differentiation. The yellow-dotted regions 1 (WT) and 2 (myosin KO) are enlarged to depict the cellular behavior during the initial nucleokinesis event, and the yellow-dotted regions 3 (WT) and 4 (myosin KO) are enlarged to depict the cellular behavior during the later nucleokinesis events to reposition the nucleus to the cellular front. N=3 replicates, 119 (WT) and 94 (myosin KO) cells.

B. Quantification of the nucleus-MTOC axis configuration before, during, directly after, and later after amoeboid nucleokinesis in myosin-IIA KO or control DCs at day 8 of differentiation (1=all cells position the nucleus in front of the MTOC; -1= all cells position the MTOC in front of the nucleus). Data are mean±95CI, Mann-Whitney test, N=3 replicates, 119 (control) and 94 (myosin KO) cells, and 1813 (before; control), 1511 (before; KO), 617 (into a dead end, control), 555 (into a dead end, KO), 286 (out of a dead end, control), 282 (out of a dead end, KO), 468 (directly thereafter, control), 411 (directly thereafter, KO), 1953 (later thereafter, control), and 1700 (later thereafter, KO) image frames.

C. Heatmap of the nucleus-MTOC axis configuration during amoeboid nucleokinesis in myosin-IIA KO or control DCs at day 10 of differentiation. The yellow-dotted regions 1 (WT) and 2 (myosin KO) are enlarged to depict the cellular behavior during the initial nucleokinesis event, and the yellow-dotted regions 3 (WT) and 4 (myosin KO) are enlarged to depict the cellular behavior during the later nucleokinesis events to reposition the nucleus to the cellular front. N= 3 replicates, 92 (WT) and 49 (myosin KO) cells.

D. Quantification of the nucleus-MTOC axis configuration before, during, directly after, and later after amoeboid nucleokinesis in myosin-IIA KO or control DCs at day 10 of differentiation (1=all cells position the nucleus in front of the MTOC; -1= all cells position the MTOC in front of the nucleus). Data are mean±95CI, Mann-Whitney test, N=3 replicates, 92 (control) and 49 (myosin KO) cells, and 1294 (before; control), 1000 (before; KO), 441 (into a dead end, control), 331 (into a dead end, KO), 208 (out of a dead end, control), 186 (out of a dead end, KO), 346 (directly thereafter, control), 311 (directly thereafter, KO), 1233 (later thereafter, control), and 1056 (later thereafter, KO) image frames.

Appendix Figure S6. Slower retractions of nucleus-containing protrusions in Lfc knockout DCs.

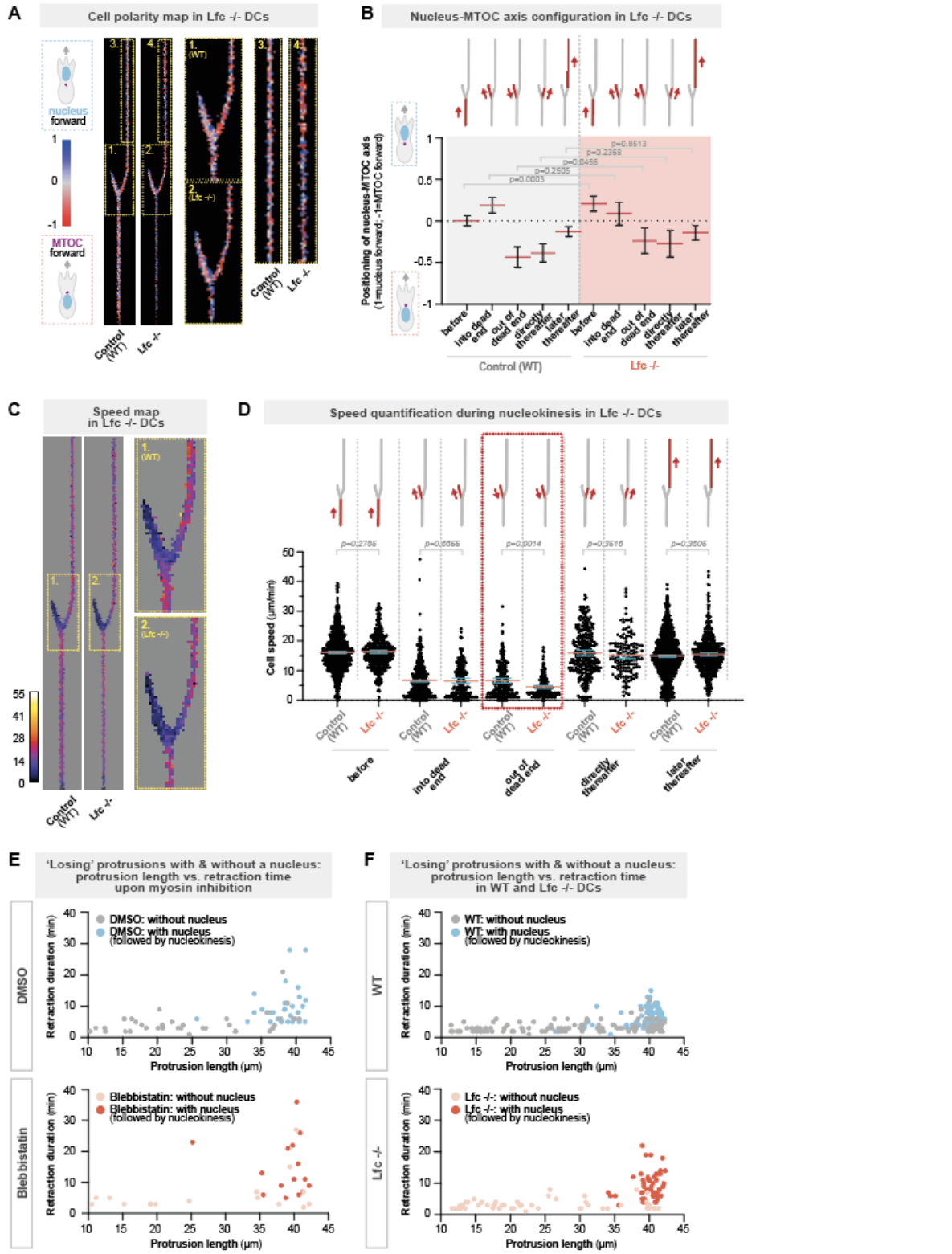

Appendix Figure S6. Slower retractions of nucleus-containing protrusions in Lfc -/- DCs.

A. Comparable nucleus-MTOC axis configuration in Lfc knockout cells to WT cells during amoeboid nucleokinesis: the MTOC was visualized by spy-tubulin; Data shows heatmaps of the nucleus-MTOC axis configuration during amoeboid nucleokinesis in WT and Lfc -/- DCs. The yellow-dotted regions 1 (WT) and 2 (Lfc -/-) are enlarged to depict the cellular behavior during the initial nucleokinesis event, and the yellow-dotted regions 3 (WT) and 4 (Lfc -/-) are enlarged to depict the cellular behavior during the later nucleokinesis events to reposition the nucleus to the cellular front. N=4 replicates, 105 (WT) and 42 (Lfc -/-) cells.

B. Quantification of A) of the nucleus-MTOC axis configuration before, during, directly after, and later after amoeboid nucleokinesis in Lfc -/- or WT cells (1=all cells position the nucleus in front of the MTOC; -1= all cells position the MTOC in front of the nucleus). Data are mean±95CI, Mann-Whitney test, N=4 replicates, 105 (WT) and 42 (Lfc -/-) cells, and 1029 (before; WT), 439 (before; Lfc -/-), 424 (into a dead end, WT), 198 (into a dead end, Lfc -/-), 212 (out of a dead end, WT), 160 (out of a dead end, Lfc -/-), 290 (directly thereafter, WT), 143 (directly thereafter, Lfc -/-), 1084 (later thereafter, WT), and 480 (later thereafter, Lfc -/-) image frames.

C. Heatmap of nuclear speed during amoeboid nucleokinesis in Lfc -/- or WT cells. The yellow-dotted regions 1 (WT) and 2 (Lfc -/-) are enlarged to depict the cellular behavior during the initial nucleokinesis event. N= 4 replicates, 105 (WT) and 42 (Lfc -/-) cells.

D. Quantification of C) of the nuclear speed during amoeboid nucleokinesis in Lfc -/- or WT cells. N= 4 replicates, 113 (WT) and 52 (Lfc -/-) cells, total analyzed events per column are 1029 (before; WT), 439 (before; Lfc -/-), 424 (into a dead end, WT), 198 (into a dead end, Lfc -/-), 212 (out of a dead end, WT), 160 (out of a dead end, Lfc -/-), 290 (directly thereafter, WT), 143 (directly thereafter, Lfc -/-), 1084 (later thereafter, WT), and 480 (later thereafter, Lfc -/-); data are mean±95CI, Mann-Withney test.

E. Correlating the retraction time of 'losing' protrusions vs their length, comparing 'losing' protrusions without a nucleus and with a nucleus upon myosin inhibition by para-nitroblebbistatin vs controls (DMSO). N= 5 replicates, 38 cells (DMSO, without nucleus), 29 (DMSO, with nucleus), 17 cells (blebbistatin, without nucleus) and 29 cells (blebbistatin, with nucleus). See also main figure 5E for quantification of retraction times of 'losing' protrusions with and without a nucleus upon myosin inhibition.

F. Correlating the retraction time of 'losing' protrusions vs their length, comparing 'losing' protrusions without a nucleus and with a nucleus in WT and Lfc -/- DCs. N= 4 replicates, 113 cells (WT, without nucleus), 113 (WT, with nucleus), 52 cells (Lfc -/-, without nucleus) and 52 cells (Lfc -/-, with nucleus). See also main figure 5F for quantification of retraction times of 'losing' protrusions with and without a nucleus in Lfc -/- DCs.

Appendix Figure S7. Delayed nucleokinesis upon myosin inhibition in *Dictyostelium*.

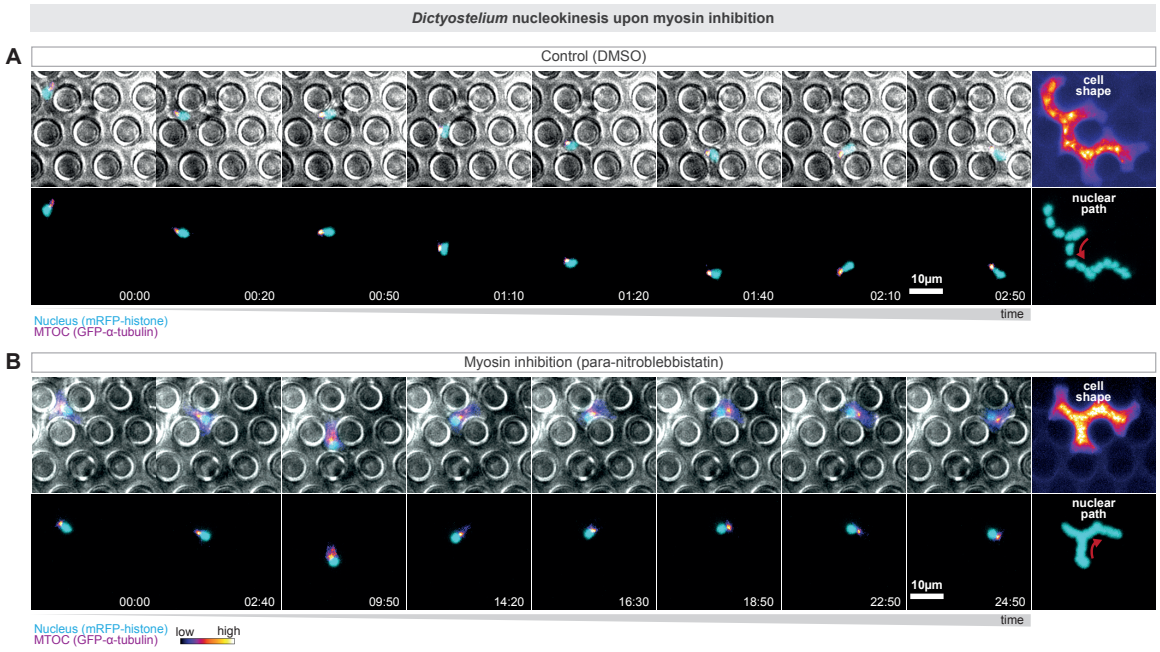

Appendix Figure S7. Delayed nucleokinesis upon myosin inhibition in *Dictyostelium*.

A. Representative *Dictyostelium* cell (control: DMSO) migrating in a pillar maze. The *Dictyostelium* cell stably encodes GFP-α-tubulin, which also visualizes the microtubule-organizing center (MTOC; in pink) and mRFP-histone, which visualizes the nucleus (in cyan). Projections of cellular (fire) and nuclear (blue) paths are shown on the right. The red arrow highlights the nucleokinesis event. Time in min:sec.

B. Representative *Dictyostelium* cell migrating in a pillar maze upon myosin inhibition (25 µM para-nitroblebbistatin). The *Dictyostelium* cell stably encodes GFP-α-tubulin, which also visualizes the microtubule-organizing center (MTOC; in pink) and mRFP-histone, which visualizes the nucleus (in cyan). Projections of cellular (fire) and nuclear (blue) paths are shown on the right. The red arrow highlights the nucleokinesis event. Time in min:sec.